

ORIGINAL ARTICLE

**Hydrodynamic effects of spines:
A different spin**Hoa Nguyen,¹ Lee Karp-Boss,² Peter A. Jumars,² and Lisa Fauci³**Abstract**

Many small planktonic organisms bear spines, some of whose potential functions have been explored, for example, in increasing drag during gravitational settling or in defense against predators. Using an immersed boundary framework, we performed computational fluid dynamic simulations that examine the rotational dynamics of model diatoms in shear flows with varying spine number, length, and angle. We found that the motion of spined cells could be accurately predicted from simple theory for motion of spheroids by applying that theory to the smallest spheroid that could inscribe the cell inclusive of its spines. The poorest fits were for small numbers or extreme angles of spines that left large volumes of the inscribing spheroid unoccupied by any spines. Although the present work provides a simple means of predicting motions of rigid, spined cells in shear flows, the effects of spines on nutrient exchange remain to be explored.

Keywords: diatoms, immersed boundary method, Jeffery orbits, phytoplankton, shear flow

Introduction

[1] Spines and other cell projections are common and notable features in vegetative cells and cysts of several groups of phytoplankton (Thomas 1997). These structures, which can be several times longer than the diameter of the cell, substantially increase the effective size of the cell with relatively little addition of mass. Various functions or adaptive values that are not mutually exclusive have been posited for such features in small plankton belonging to diverse protist and animal taxa. Depending on the balance between added drag and added excess density, spines and other protuberances can slow gravitational settling (Furbish and Arnold 1997; Padisák et al. 2003) and can serve as defense mechanisms against grazers (Stemberger and Gilbert 1984). Some laboratory experi-

ments, however, have shown higher filtration rates on cells with spines than on cells of the same species that lack spines (Gifford et al. 1981), presumably because the added length or altered behavior of spined cells in feeding currents may increase the encounter rate with predators.

[2] In a seminal paper, Jeffery (1922) used the ratio of the two different axis lengths describing a spheroid to predict the rate at which spheroidal particles tumble when placed in uniform, steady shear. Consequences of such tumbling are significant because cell encounters with molecules of nutrients and infochemicals and with neighboring cells and grazers all depend on the differential motion of the cell from its surrounding fluid (Karp-Boss et al. 1996; Kjørboe 2008). Diffusion is enhanced during

¹Center for Computational Science, Tulane University, New Orleans, Louisiana 70118, USA

²School of Marine Sciences, University of Maine, Orono, Maine 04469, USA

³Mathematics Department, Tulane University, New Orleans, Louisiana 70118, USA

Correspondence to
Lisa Fauci,
fauci@tulane.edu

tumbling not by any particular orientation but by rapid change in orientation that causes fluid exchange near the cell (Pahlow et al. 1997; Musielak et al. 2009).

[3] Spines are expected to affect such motions of organisms in natural flows because they can markedly change the aspect ratio of the cell, literally levering it. In an in vivo laboratory study, rigid chains of diatoms in a simple shear flow moved approximately as predicted by Jeffery (1922), but the motion of flexible chains with spines deviated from theoretical predictions (Karp-Boss and Jumars 1998). To represent a common spine morphology, we chose the diatom genus *Thalassiosira*, which is widespread in the world's oceans. Cells are discoidal or cylindrical, and external siliceous tubes (spines) project from each valve (Fig. 1). The tubes are arranged in a ring around the rim of the valve or in groups on the valve face, with considerable variation within the genus (Round et al. 1990). Organic threads may be extruded from the tube, but in this first study we represented spines and the cell as being rigid. Also for simplicity, we refer to all cell projections as spines even though a variety of terms has been used in the literature to de-

scribe these structures (Zugger et al. 2008). We expected spines to affect cell motion in natural flows because, at low particle Reynolds numbers, flow perturbations propagate large distances and because drag of slender bodies such as spines depends strongly on their orientation to the flow. We therefore undertook a numerical study to examine how the number, length, and orientation of spines affect the motion of a discoidal cell in a flow. We focused on a simple shear flow because of its predominance in past experiments and because verified predictive theory exists for spheroids (Jeffery 1922).

Methods

[4] We solved the full, three-dimensional Navier-Stokes equations that govern incompressible, viscous flow to model the dynamics of a cell moving in a shear flow. We used an immersed boundary framework (Peskin 1977, 2002) to capture the interaction of the complex cell geometry with the surrounding fluid. The surfaces of the cell and associated spines were discretized as a network of points connected mechanically by virtual “springs.” For these first models, spring stiffnesses

were chosen large enough so that the cell did not deform in response to the moving fluid. We employed an adaptive and parallel implementation of the immersed boundary method, IBAMR (Griffith et al. 2007), to compute flow near the cell with high resolution.

[5] We validated our numerical approach by checking whether a modeled ellipsoid immersed in a shear flow behaved as predicted by theory (Jeffery 1922) and whether the period of rotation of a modeled flat disk immersed in a shear flow agreed with experimental

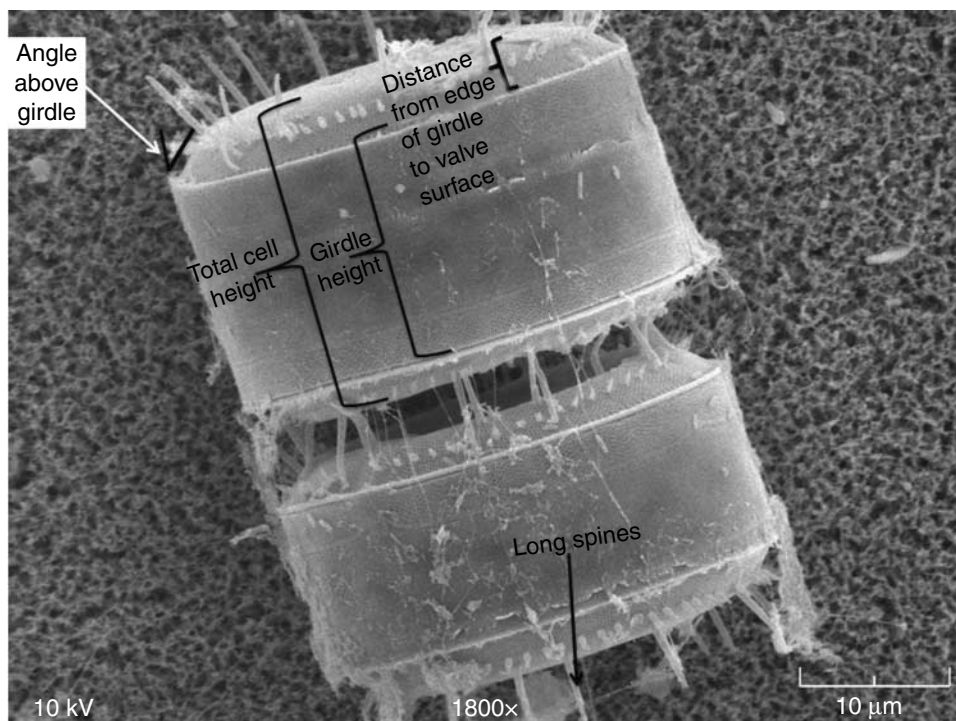


Fig. 1 *Thalassiosira punctigera*: image of two cells by A. M. Young (for detailed measurements, see Table 2).

results (Goldsmith and Mason 1962). We examined how the addition of spines to the flat disk model altered cell motion in the same simple shear flows.

Spheroid in Shear Flow

[6] A spheroid is an axisymmetric ellipsoid with two principal axes of equal length. We constructed a model spheroid by first tessellating a sphere to create a grid (surface triangulation) that satisfied the conditions of uniformity and robust discretization at various scales, using spherical centroidal Voronoi tessellation (Du et al. 1999, 2003). We mapped the surface triangulation of a unit sphere onto a spheroid surface (Fig. 2A). To maintain the shape of the spheroid, we connected adjacent points on the surface of the spheroid with virtual linear springs on the edges of the triangulation. The force between two connected points (\mathbf{x}_k and \mathbf{x}_l) was computed as

$$\mathbf{f}(\mathbf{x}_k) = \tau_k \left(1 - \frac{\delta_k}{\|\mathbf{x}_l - \mathbf{x}_k\|} \right) (\mathbf{x}_l - \mathbf{x}_k), \quad (1)$$

where τ_k is a stiffness constant of the linear spring, δ_k is its resting length, the distance between \mathbf{x}_l and \mathbf{x}_k when the surface is initialized at time $t = 0$, and $\|\mathbf{x}_l - \mathbf{x}_k\|$ represents the Euclidean norm, that is, the positive distance between the two points.

[7] The spheroid Γ was modeled as a neutrally buoyant, elastic surface immersed in a viscous, incompressible fluid (where Ω is the fluid domain). The full Navier-Stokes equations were solved, where the force term \mathbf{F} represents the force per unit of volume exerted

on the fluid by the spheroid,

$$\rho \left[\frac{\partial \mathbf{u}}{\partial t} + \mathbf{u} \cdot \nabla \mathbf{u} \right] = -\nabla p + \mu \Delta \mathbf{u} + \mathbf{F}(\mathbf{x}, t), \quad (2)$$

$$\nabla \cdot \mathbf{u} = 0, \quad (3)$$

$$\mathbf{F}(\mathbf{x}, t) = \int_{\Gamma} \mathbf{f}(s, t) \delta(\mathbf{x} - \mathbf{X}(s, t)) ds, \quad (4)$$

with the no-slip condition

$$\frac{\partial \mathbf{X}(s, t)}{\partial t} = \mathbf{u}(\mathbf{X}(s, t), t) = \int_{\Omega} \mathbf{u}(\mathbf{x}, t) \delta(\mathbf{x} - \mathbf{X}(s, t)) d\mathbf{x}. \quad (5)$$

Here ρ is fluid density, \mathbf{u} is fluid velocity, p denotes pressure, μ is dynamic viscosity, and s denotes Lagrangian coordinates attached to the immersed elastic boundary Γ . The Eulerian force density \mathbf{F} on the fluid is a Dirac delta-function δ layer of elastic forces \mathbf{f} supported by the triangular elements of the spheroid surface (refer to equation (4)). In other words, this force is experienced only by fluid that touches the spheroid surface. Away from these points, the force of the spheroid on the fluid is zero.

[8] According to Jeffery’s theory, a spheroid suspended in a simple shear flow at a vanishing Reynolds number rotates in a stable orbit independent of its initial orientation. The orbit can be described by changes in azimuthal angle Φ over time, where Φ is the angle in the x,z -plane between the spheroid’s major axis and the positive z -axis ($0 \leq \Phi \leq 2\pi$). According to Jeffery (1922), $\Phi = \tan^{-1}(a_r \tan(2\pi(t/T)))$, where a_r is the axis ratio (the ratio of the axis of rotation and the

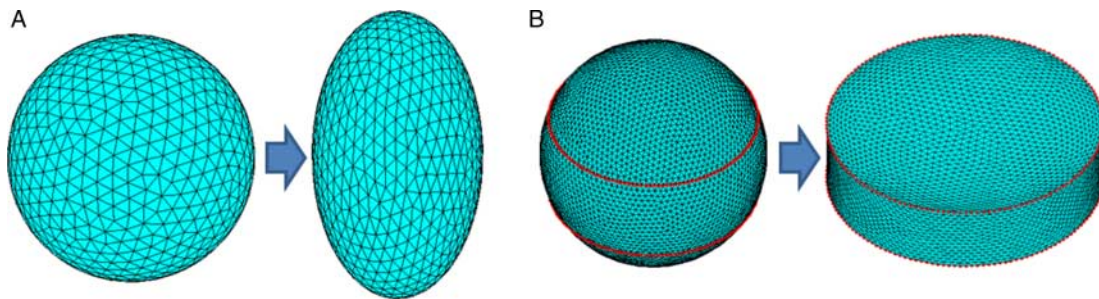


Fig. 2 Mapping of the spherical centroidal Voronoi tessellation on (A) a unit sphere to a spheroid and (B) a unit sphere to a flat disk (the red points on the sphere mapping to the edges of the top and bottom of the disk).

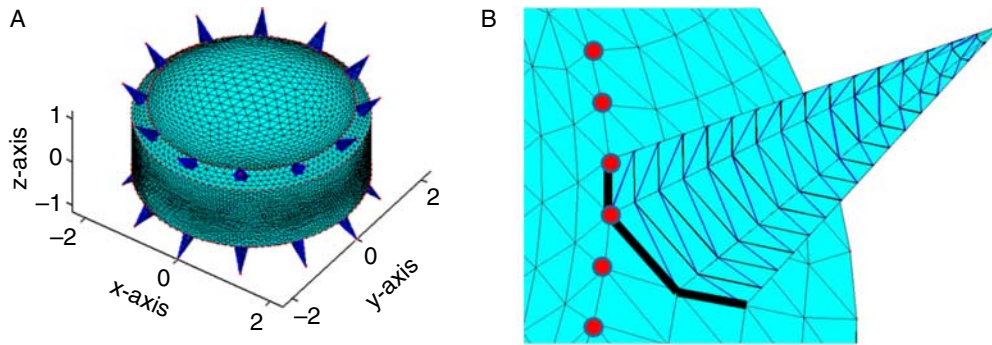


Fig. 3 (A) A simplified model of a diatom cell with 24 spines; dimensions ($\times 10^{-5}$ m) are based on measurements provided in Table 2. (B) Magnified view near the base of a spine (red dots indicate the rim of the valve surface).

equatorial axis) and T is the period of rotation of the spheroid. The latter is given by $T = 2\pi/\gamma(a_r + (1/a_r))$, where γ is the shear rate (Jeffery 1922). To validate our code, we compared changes in the azimuthal angle and periods of rotation predicted by theory to the values obtained from our model of an ellipsoid. The major axis of the spheroid (the axis of rotation) was orthogonal to the flow direction at $t = 0$, and thus motion of this axis will remain in a plane. Whereas these calculations are fully three-dimensional and work with any initial orientation, we chose to focus on the planar rotation to minimize the complexity of our model results.

Flat Disk in Shear Flow

[9] Although Jeffery orbit theory is restricted to spheroids, computational models carry no such restrictions. In order to gain confidence in our calculations for complex diatom geometries with spines, we examined the rotational dynamics of a flat disk in a shear flow. We compared our computed periods of rotation of modeled flat disks with experimental results (Goldsmith

and Mason 1962). In this case, the surface triangulation of a unit sphere was mapped onto the surface of a flat disk (Fig. 2B). As with the spheroid, the flat disk was placed in the middle of a shear flow field, with model viscosity matching that used in Goldsmith and Mason's

(1962) experiments with silicone oil. The axis of the flat disk was set orthogonal to the flow at $t = 0$.

Model of a Diatom with Spines in Shear Flow

[10] We constructed a model cell of the diatom (Fig. 3A, Table 1) based on measured dimensions from electron microscope images of *Thalassiosira punctigera* cells that we grew in the lab (Fig. 1, Table 2). When we discretized the cell body with triangular meshes, we positioned fixed points near the valve surfaces to place the centerlines of the spines. The neighboring triangles that share the fixed point as one of their vertices form the base of the spine, which has a pyramidal shape (Fig. 3B). The axis of the plankter disk (squat cylinder) was set orthogonal to the flow at $t = 0$.

[11] An important question that we want to address is whether Jeffery's (1922) theory for spheroids can accurately approximate the rotational motion of a cell with spines, thereby allowing simple computations of cell motions in flows. We postulated that the

Table 1 Characteristic quantities for the spheroid, flat disk, and model diatom.

Characteristic quantity	Spheroid	Flat disk	Model diatom
Fluid domain size in each direction (m)	4.0×10^{-3}	8.0×10^{-3}	2.8×10^{-4}
Length of the equatorial axes (diameter of the disk or diatom) (m)	9.0×10^{-5}	8.0×10^{-4}	4.25×10^{-5}
Length of the axis of rotation (height of the diatom) (m)	18.2×10^{-5}	2.0×10^{-4}	1.77×10^{-5}
Shear rate (s^{-1})	10.0	2.43	10.0
Reynolds number (dimensionless)	3.3×10^{-1}	3.0×10^{-4}	1.8×10^{-2}
Fluid density ($kg\ m^{-3}$)	10^3	975.0	10^3
Dynamic viscosity (Pa s)	10^{-3}	5.0	10^{-3}
Stiffness constant ($N\ m^{-1}$)	2.0×10^{-3}	10^{-1}	5.0×10^{-5}

Table 2 Dimensions of *Thalassiosira punctigera* obtained from scanning electron microscope images by A. M. Young.

Parameter	Mean \pm SD ($\times 10^{-6}$ m)	Sample size
Diameter	42.5 \pm 9.7	6
Girdle height	15.5 \pm 3.4	8
Distance from edge of girdle to valve surface	2.2 \pm 0.7	2
Total cell height	18.5 \pm 4.2	8
# of long spines (one side)	12.0 \pm 4.0	3
Length of long spines	4.9 \pm 1.0	8
Diameter of spines	0.84 \pm 0.22	5
Distance of long spines from edge of girdle	4.1 \pm 1.1	4
Distance of long spines from each other	7.1 \pm 1.3	4
Angle above girdle (degrees)	49.1 \pm 2.6	3

minimum-volume spheroid that can inscribe the cell inclusive of its spines would most closely approximate its orbit (period of rotation). Depending on spine length and orientation, the minimum-volume spheroid can be oblate or prolate (Fig. 4). The procedure for finding it is detailed in the Appendix.

Results

Validation of the Models

[12] We performed computational simulations that examined the rotational dynamics of the spheroid and flat disk in a shear flow, using the parameters in Table 1. The Reynolds number (Re) of the resulting flow is computed as $Re = \rho\gamma L^2/\mu$, where L is the characteristic length. For the spheroid, L is the length of the axis of

rotation ($Re = 3.3 \times 10^{-1}$), and for the flat disk, it is the diameter of the disk ($Re = 3.0 \times 10^{-4}$).

[13] Changes in the azimuthal angle of the modeled spheroid, determined by tracking the trajectories of the material points that discretize the surface of the spheroid as it rotates in the background shear flow, follow closely the changes predicted by Jeffery's theory (Fig. 5A). The period of rotation of the modeled spheroid also agreed well with the theoretical prediction (1.5872 and 1.5867 s, respectively). The deviation was smaller than the variance observed for replicate trials in experimental determinations, which are usually reported to only two significant figures.

[14] We examined the sensitivity of our results for a modeled diatom to variations in the resolution of the underlying fluid grid. For this convergence study, we chose a diatom with 24 spines and ran the models using either two or three levels of grid refinement in the adaptive computational method. The coarsest grid level used in the fluid domain away from the diatom was 2.0×10^{-5} (two refinement levels) and 1.75×10^{-5} m (three refinement levels). In particular, the finest grid spacing that was achieved between the spines was 5.0×10^{-6} m (two refinement levels) and 1.09×10^{-6} m (three refinement levels). For reference, the diameter of the cell body is 4.25×10^{-5} m, and the distance between spines at the base is approximately 5.6×10^{-6} m. Fig. 5B shows the time course of the azimuthal angle for the diatom at each of these levels of refinements as a function of time; the rotational trajectories of the spined diatoms are very close at these resolutions.

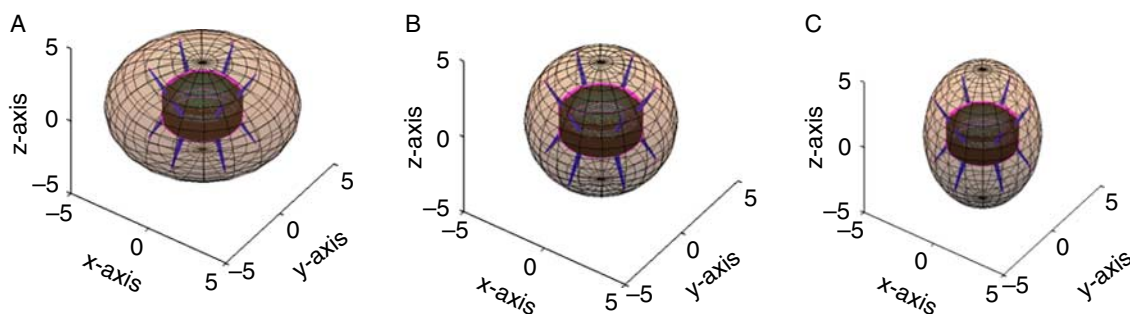


Fig. 4 A cell modeled using different spheroids: (A) oblate spheroid, (B) spheroid with minimum volume, and (C) prolate spheroid (dimensions in $m \times 10^{-5}$). Colors are for visual contrast.

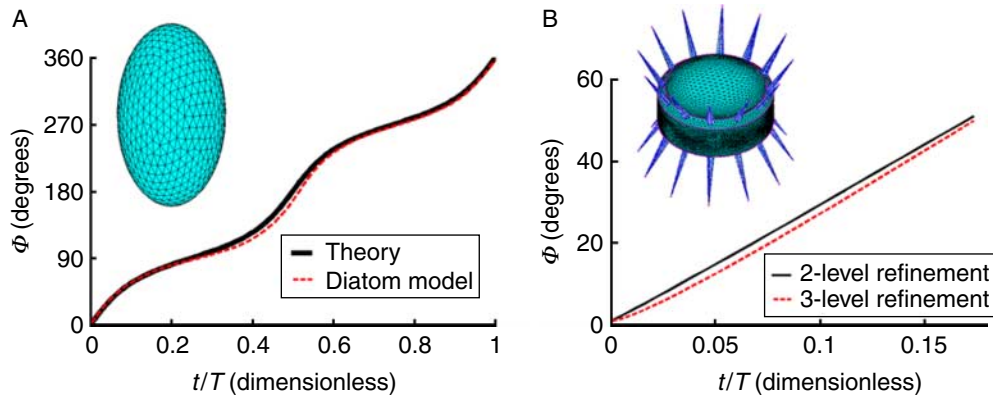


Fig. 5 Variation of the azimuthal angle, Φ , of (A) a spheroid and (B) a diatom with spines, as a function of time, t , scaled by the rotational period, T . The two trajectories in B correspond to the levels of grid refinement used in solving the Navier-Stokes equations.

Model of a Diatom with Spines in Shear Flow

[15] Using the characteristic quantities in Table 1, we modeled a diatom in a shear flow to examine the effects of spine number and length on the period of rotation.

Effect of the Number of Spines on the Period of Rotation

[16] To address our first question about the effect of the number of spines on the period of rotation, we fixed spine angle and length at intermediate values of 60° and 1.80×10^{-5} m, respectively. We varied the number of spines from 4 to 24. In general, published, quantitative information on spine number and dimension is scarce. The range of number of spines chosen here is based on available images of different species of spiny diatoms of the genera *Thalassiosira*, *Corethron*, and *Chaetoceros*. For a given spine length and spine angle, the addition of spines decreased the period of rotation very little (see Table 3, where T_{sim} is the computed period of rotation). Note that since only the number of spines was varied, the modeled diatoms have the same minimal inscribing spheroid whose period of rotation is 1.27 s.

Effect of Spine Length on the Period of Rotation

[17] To examine whether spine length affects the period of rotation, we fixed the number of spines at 24 (i.e., 12 spines each on top and bottom) and the spine angle at 60° and varied spine length. We used the minimal inscribing spheroids to compare their Jeffery orbits T_{sph} with the computed periods of the diatoms T_{sim} . In this case, the minimal inscribing spheroid also minimized the difference in periods of rotation in comparison with larger inscribing spheroids (Fig. 6). The addition of short spines resulted in a decrease in the period of rotation, compared with a spineless cell, until a critical spine length was reached. A further increase in spine length slowed the rotation, but the period of rotation was still shorter than that of the cell without spines. For the given fixed spine angle and spine number, the period of rotation of the cell can be approximated by an effective spheroid (Fig. 6).

[18] Based on the formula used to compute the period of rotation

$$\left(T = \frac{2\pi}{\gamma} \left(a_r + \frac{1}{a_r} \right) \right), \quad (6)$$

it is clear that a sphere with $a_r = 1$ has the shortest

Table 3 Period of rotation (T_{sim}) for model diatoms with different number of spines (spine angle 60° and spine length 1.80×10^{-5} m).

Number of spines	0	4	6	8	12	18	24
T_{sim} (s)	1.40	1.29	1.29	1.29	1.29	1.28	1.28

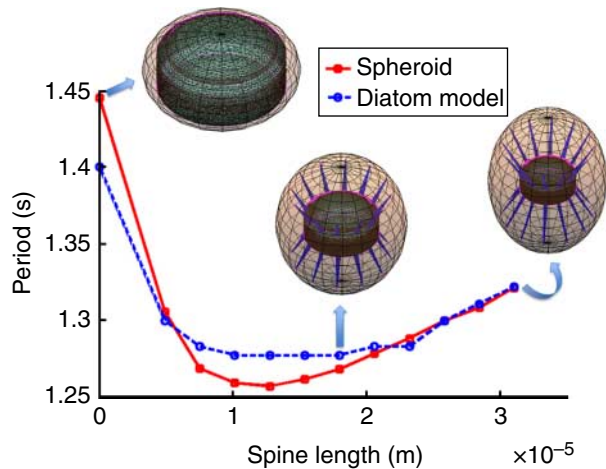


Fig. 6 Effect of spine length on the period of rotation of the model diatom compared with the minimal-volume inscribing spheroid.

period. When the minimal inscribing spheroid is a sphere or nearly spherical, the period of the corresponding plankter is also smallest (Fig. 6, Table 4). Note that the axis ratio of the minimal inscribing spheroid depends on four factors: height of the cell body, diameter of the cell body, spine length, and spine angle. For a diatom with short spines relative to the body dimensions, the spheroid axis ratio will depend more heavily on the ratio of body height to diameter (the spines will have less influence over the shape of the spheroid). If the spines are long relative to the body, then spine angle becomes more important in governing the axis ratio of the spheroid.

Effect of Spine Angle on the Period of Rotation

[19] Spine length was fixed at 1.80×10^{-5} m, and spine angle was varied for three spine densities (4, 12, and 24

Table 4 The effect of spine length on the period of rotation of minimum-volume inscribing spheroids (T_{sph}), the corresponding period for model diatoms (T_{sim}), and the axis ratio (a_r).

Spine length ($\times 10^{-5}$ m)	0.00	0.49	0.75	1.01	1.28	1.54
T_{sim} (s)	1.40	1.30	1.28	1.28	1.28	1.28
T_{sph} (s)	1.45	1.31	1.27	1.26	1.26	1.26
a_r	0.58	0.76	0.87	0.94	1.00	1.09
Spine length ($\times 10^{-5}$ m)	1.80	2.06	2.32	2.58	2.84	3.11
T_{sim} (s)	1.28	1.28	1.28	1.30	1.31	1.32
T_{sph} (s)	1.27	1.28	1.29	1.30	1.31	1.32
a_r	1.14	1.20	1.25	1.30	1.33	1.38

spines per cell). Results from these models suggest that spine angle affects the period of rotation only at small angles ($< 30^\circ$) and that the effect becomes more pronounced as spine number increases (Fig. 7). For this range of angles, and for angles approaching 90° , the period of rotation of a cell with spines cannot be approximated well by Jeffery’s theory for spheroids. The poorest agreement between the modeled cell and the minimal inscribing spheroid was observed when angles were at their most extreme, 0 and 90° (Fig. 7).

Discussion

[20] The average period of rotation of the modeled disk was slightly lower than that obtained in Goldsmith and Mason’s (1962) laboratory experiments (6.5 and 7.6 s, respectively). For reference, the predicted period of rotation for a spheroid with the same height and diameter is $T = 11$ s (Jeffery 1922). Sharp edges on modeled and manufactured cylinders and disks reduce their periods of rotation relative to smoother spheroids of comparable aspect ratios (Karp-Boss and Jumars 1998).

[21] The fit of our numerical results to Jeffery orbits of spheroids and to experimental results for disks indicates that the underlying computational approach is sound. The addition of stiff spines to a disk has a substantial effect on its period of rotation. Results from these models suggest that the bulk of the variation in rotational frequency in shear can be predicted by

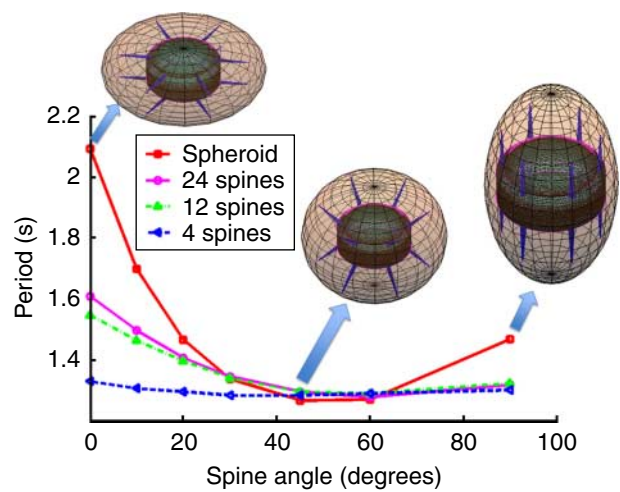


Fig. 7 Effect of spine angle on the periods of rotation of a model diatom with 4, 12, and 24 spines compared with the minimal inscribing spheroid.

using results for the minimum-volume, rigid spheroid that inscribes the cell and its spines. Spines facilitate motion that would otherwise be associated with a change in shape (i.e., rotational frequency), without changing the underlying body shape and with substantially less material than would be needed to fill the inscribing spheroid. Not surprisingly, the minimal inscribing spheroid showed poorest fits when small numbers or extreme angles of spines left large volumes of the inscribing spheroid unoccupied by spines.

[22] These results are reminiscent of those explored by Hill and Power (1956). They proved a theorem that no matter how complex an object's geometry, its drag in Stokes (creeping) flow must be larger than that of any inscribed object but smaller than that of any circumscribing object. Hence, the drag on our minimal inscribing spheroid gives an upper bound on the total drag on the spined diatom relative to the lower drag on an unspined cell. Consequently, the rich literature on motion and drag of spheroids (e.g., Clift et al. 1978; Happel and Brenner 1983; Kim and Karilla 1991) should provide a rich resource for anticipating motions by and forces on bodies of complex shapes.

[23] Although overall body motion is simple to summarize, especially for intermediate to large numbers of spines and moderate spine angles, consequences for nutrient exchange may be more complex. Spines may substantially alter the relative motion of the fluid in the regions closest to the valve surface where concentration gradients from uptake or release of diffusing solutes are steepest. If they carry no absorptive sites, we would expect spines to reduce the effective Sherwood number (the ratio of advective to diffusive flux) for nutrient delivery relative to the same cell without spines. Cell motion, however, will be altered by the spines. The delivery of nutrients to spined cells remains to be explored, but the Hill and Power (1956) results suggest that an upper bound on delivery could be calculated as that of a minimum-volume, inscribing, spheroidal absorber.

[24] It is relevant to note that the cells investigated were radially symmetric and also bilaterally (or reflectively) symmetric about the midpoint of their radial

axis. Poorer fits to the spheroidal approximation and more diverse motions can be expected with departures from these symmetries. Our results also highlight the need to examine the topology of absorptive surfaces on the cell in order to understand the degree to which spines may restrict fluid motion close to the cell body and thereby reduce the potential for nutrient gain from tumbling motions (Pahlow et al. 1997; Musielak et al. 2009). Because of the complex geometries, such understanding likely will come through further numerical modeling. Our results are also limited to rigid, passive particles. More complex interactions between flow and structure will result when structures are flexible enough to be bent by ambient flows. These interactions remain accessible to immersed boundary methods, where the stiffness parameters used in the model may be matched to stiffness *in vivo*. The effects of ambient flow on spined, motile plankton, such as species in the dinoflagellate genus *Ceratium*, also remain to be examined but may provide a partial explanation of its seasonal cyclo-morphosis in some environments (Dodson 1974).

Significance to Aquatic Environments

[25] Relations between form and function in the diverse morphologies found in plankton remain challenging to decipher. We identified a surprisingly simple means to approximate the motion of complexly shaped cells by using the minimum-volume, inscribing spheroid to predict Jeffery orbits (i.e., the motion that an ellipsoidal particle undergoes in shear flow). This simple solution should prove useful for predicting trophic encounters in shear flows produced by grazers (e.g., Visser and Jonsson 2000) and cell-cell encounters in shear coagulation (e.g., Kiørboe et al. 1994). Although our models of single cells do not quantify this effect, plankton span a broader range of flow velocities and present larger cross-sectional areas to the flow when they tumble and thus should be more prone to coagulation and other encounters. This methodology should also be useful for predicting fluid torques on spined bodies whose spines are induced as predator defense mechanisms. Those torques applied by ambient turbulent flows may represent costs

additional to the known effects of induced spines on drag during swimming (e.g., Lagergren et al. 1997).

Appendix

How to Find an Associated Spheroid for a Given Diatom

[A1] Assume that the discoidal cell body of a diatom has diameter a and height b . Let $r = a/2$ and $h = b/2$. We denote l as the spine length from the tip to the base and α as the angle between the spine and the girdle plane. Associate the spined diatom with a spheroid (either oblate or prolate; Fig. A1), where \bar{a} is half of the length of the spheroid along the x -axis and \bar{b} is half of the length of the spheroid along the z -axis.

[A2] The spheroid must satisfy the following conditions: (a) the tips of the diatom spines are on the surface of the spheroid, and (b) the foci of the spheroid are on the plane equidistant from the top and bottom surfaces of the diatom. Denote this spheroid as an oblate spheroid (see Fig. A1A). If the foci are placed along the axis of the cylindrical cell, the spheroid is a prolate spheroid (see Fig. A1B).

[A3] For the oblate spheroid, we can simplify this problem by finding an ellipse on the x,z -plane such that the foci are $F_1 = (-\beta r, 0)$, $F_2 = (\beta r, 0)$ with $\beta \geq 0$ and $|\overline{PF_1}| + |\overline{PF_2}| = 2\bar{a}$ (where P represents the tip of a spine). β is a nonnegative real parameter used to adjust the distances of the foci from the center of the ellipse ($\beta = 0$ returns a sphere). Then

$$\bar{a} = \frac{1}{2} \sqrt{r^2(1 + \beta)^2 + h^2 + l^2 + 2l[r(1 + \beta)\cos\alpha + h\sin\alpha]} + \frac{1}{2} \sqrt{r^2(1 - \beta)^2 + h^2 + l^2 + 2l[r(1 - \beta)\cos\alpha + h\sin\alpha]} \tag{A1}$$

As a result, half of the length of the minor axis (along the z -axis) is

$$\bar{b} = \sqrt{\bar{a}^2 - (\beta r)^2} \tag{A2}$$

Similarly, for the prolate spheroid with the foci $F_1 = (0, -\beta h)$, $F_2 = (0, \beta h)$ with $\beta \geq 0$, half of the length of the major axis along the z -axis is:

$$\bar{b} = \frac{1}{2} \sqrt{h^2(1 + \beta)^2 + r^2 + l^2 + 2l[h(1 + \beta)\sin\alpha + r\cos\alpha]} + \frac{1}{2} \sqrt{h^2(1 - \beta)^2 + r^2 + l^2 + 2l[h(1 - \beta)\sin\alpha + r\cos\alpha]} \tag{A3}$$

As a result, half of the length of the minor axis (along x -axis) is

$$\bar{a} = \sqrt{\bar{b}^2 - (\beta h)^2} \tag{A4}$$

How to Find the Minimum-Volume Spheroid for a Given Diatom

[A4] The above section shows how to find a single inscribing spheroid for a given plankter by choosing a parameter $\beta \geq 0$. The minimum-volume spheroid is the inscribing spheroid that minimizes the difference between the volumes of itself and the plankter. Computationally, this means finding the parameter β that minimizes the volume difference; hence, the minimum-volume spheroid can be oblate or prolate.

Acknowledgments H. N. and L. F. are partially supported by National Science Foundation (NSF) OCE 0724598, and L. K.-B. and P. J. are partially supported by NSF grant OCE 0724744. We gratefully acknowledge photographs and measurements of *Thalassiosira punctigera* made by A. M. Young (School of Marine Sciences, University of Maine). We sincerely thank Dr. Boyce Griffith (New York University) for the use of his IBAMR software, and Dr. Hideki Fujioka (Center for Computational Science, Tulane University) for assistance in its implementation.

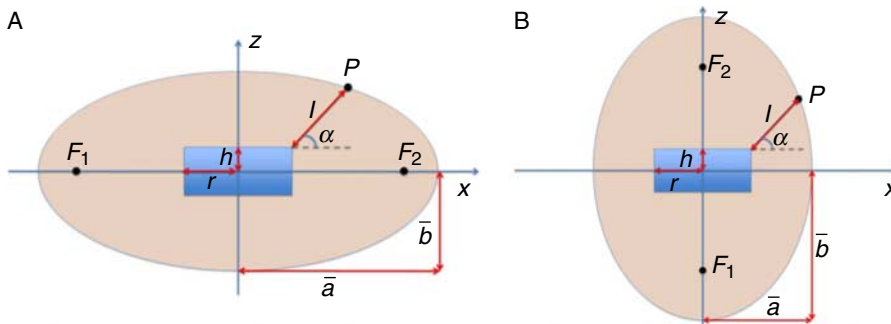


Fig. A1 A simplified, spined model enclosed by either (A) an oblate spheroid or (B) a prolate spheroid.

References

- Clift, R., J. R. Grace, and M. E. Weber. 1978. Bubbles, drops, and particles. Academic Press, Reprint, 2005. Dover.
- Dodson, S. I. 1974. Adaptive change in plankton morphology in response to size-selective predation: A new hypothesis of cyclomorphosis. *Limnol. Oceanogr.* **19**: 721–729, doi:10.4319/lo.1974.19.5.0721.
- Du, Q., V. Faber, and M. Gunzburger. 1999. Centroidal Voronoi tessellations: Applications and algorithms. *SIAM Rev.* **41**: 637–676, doi:10.1137/S0036144599352836.
- Du, Q., M. Gunzburger, and L. Ju. 2003. Constrained centroidal Voronoi tessellations for surfaces. *SIAM J. Sci. Comput.* **24**: 1488–1506, doi:10.1137/S1064827501391576.
- Furbish, D. J., and A. J. Arnold. 1997. Hydrodynamical strategies in the morphological evolution of spinose planktonic foraminifera. *Geol. Soc. Am. Bull.* **109**: 1055–1072, doi:10.1130/0016-7606(1997)109<1055:HSITME>2.3.CO;2.
- Gifford, D. J., R. W. Bohrer, and C. M. Boyd. 1981. Spines on diatoms: Do copepods care? *Limnol. Oceanogr.* **26**: 1057–1061, doi:10.4319/lo.1981.26.6.1057.
- Goldsmith, H. L., and S. G. Mason. 1962. Particle motions in sheared suspensions XIII. The spin and rotation of disks. *Fluid Mech.* **12**: 88–96, doi:10.1017/S0022112062000051.
- Griffith, B. E., R. D. Hornung, D. M. McQueen, and C. S. Peskin. 2007. An adaptive, formally second order accurate version of the immersed boundary method. *J. Comput. Phys.* **223**: 10–49, doi:10.1016/j.jcp.2006.08.019.
- Happel, J. H., and H. Brenner. 1983. *Low Reynolds Number Hydrodynamics*. Martinus Nijhoff.
- Hill, R., and G. Power. 1956. Extremum principles for slow viscous flow and the approximate calculation of drag. *Q. J. Mech. Appl. Math.* **9**: 313–319, doi:10.1093/qjmam/9.3.313.
- Jeffery, G. B. 1922. The motion of ellipsoidal particles immersed in a viscous fluid. *Proc. R. Soc. Lond. Proc. Ser. A.* **102**: 161–179, doi:10.1098/rspa.1922.0078.
- Karp-Boss, L., E. Boss, and P. A. Jumars. 1996. Nutrient fluxes to planktonic osmotrophs in the presence of fluid motion. *Oceanogr. Mar. Biol. Annu. Rev.* **34**: 71–107.
- Karp-Boss, L., and P. A. Jumars. 1998. Motion of diatom chains in steady shear. *Limnol. Oceanogr.* **43**: 1767–1773.
- Kim, S., and S. J. Karilla. 1991. *Microhydrodynamics: Principles and Selected Applications*. Butterworth-Heinemann.
- Kjørboe, T. 2008. *A Mechanistic Approach to Plankton Ecology*. Princeton University Press.
- Kjørboe, T., C. Lundsgaard, M. Olesen, and J. L. S. Hansen. 1994. Aggregation and sedimentation processes during a spring phytoplankton bloom: A field experiment to test coagulation theory. *J. Mar. Res.* **52**: 297–323, doi:10.1357/0022240943077145.
- Lagergren, R., M. Hellsten, and J. A. E. Stenson. 1997. Increased drag, and thus lower speed: A cost for morphological defense in *Bosmina (Eubosmina)* (Crustacea: Cladocera). *Funct. Ecol.* **11**: 484–488, doi:10.1046/j.1365-2435.1997.00117.x.
- Musielak, M., L. Karp-Boss, P. Jumars, and L. Fauci. 2009. Nutrient transport and acquisition by diatom chains in a moving fluid. *J. Fluid Mech.* **638**: 401–421, doi:10.1017/S0022112009991108.
- Padišák, J., É. Soróczki-Pintér, and Z. Rezner. 2003. Sinking properties of some phytoplankton shapes and the relation of form resistance to morphological diversity of plankton—an experimental study. *Hydrobiologia.* **500**: 243–257, doi:10.1023/A:1024613001147.
- Pahlow, M., U. Riebesell, and D. Wolf-Gladrow. 1997. Impact of cell shape and chain formation on nutrient acquisition by marine diatoms. *Limnol. Oceanogr.* **42**: 1660–1672, doi:10.4319/lo.1997.42.8.1660.
- Peskin, C. S. 1977. Numerical analysis of blood flow in the heart. *J. Comput. Phys.* **25**: 220–252, doi:10.1016/0021-9991(77)90100-0.
- , 2002. The immersed boundary method. *Acta Numer.* **11**: 459–517, doi:10.1017/S0962492902000077.
- Round, F. E., R. M. Crawford, and D. G. Mann. 1990. *The Diatoms: Biology and Morphology of the Genera*. Cambridge University Press.
- Stemberger, R. S., and J. J. Gilbert. 1984. Spine development in the rotifer *Keratella cochlearis*: Induction by cyclopoid copepods and *Asplanchna*. *Freshwater Biol.* **14**: 639–647, doi:10.1111/j.1365-2427.1984.tb00183.x.
- Thomas, C. R. 1997. *Identifying Marine Phytoplankton*. Academic Press.
- Visser, A., and P. R. Jonsson. 2000. On the reorientation of non-spherical prey particles in a feeding current. *J. Plankton Res.* **22**: 761–777, doi:10.1093/plankt/22.4.761.
- Zugger, M. E., A. Messmer, T. J. Kane, J. Prentice, B. Concannon, A. Laux, and L. Mullen. 2008. Optical scattering properties of phytoplankton: Measurements and comparison of various species at scattering angles between 1° and 170°. *Limnol. Oceanogr.* **53**: 381–386, doi:10.4319/lo.2008.53.1.0381.

Received: 12 October 2010

Amended: 31 December 2010

Accepted: 6 February 2011